Ultrasound in Med. & Biol., Vol. 47, No. 5, pp. 1319–1333, 2021

0301-5629/$ - see front matter

https://doi.org/10.1016/j.ultrasmedbio.2020.12.026

● *Original Contribution*

SONOPERMEATION ENHANCES UPTAKE AND THERAPEUTIC EFFECT OF FREE AND ENCAPSULATED CABAZITAXEL

Sofie Snipstad,[*,†,‡] Ýrr Mørch,[*] Einar Sulheim,[*,†,‡] Andreas Åslund,[*] André Pedersen,[§] Catharina de Lange Davies,[†] Rune Hansen,[§,¶] and Sigrid Berg[‡,§,¶]

[*] Department of Biotechnology and Nanomedicine, SINTEF Industry, Trondheim, Norway; [†] Department of Physics, Norwegian University of Science and Technology, Trondheim, Norway; [‡] Cancer Clinic, St. Olav's Hospital, Trondheim, Norway; [§] Department of Health Research, SINTEF Digital, Trondheim, Norway; and [¶] Department of Circulation and Medical imaging, Norwegian University of Science and Technology, Trondheim, Norway

(*Received* 3 *March* 2020; *revised* 18 *September* 2020; *in final from* 27 *December* 2020)

Abstract—Delivery of drugs and nanomedicines to tumors is often heterogeneous and insufficient and, thus, of limited efficacy. Microbubbles in combination with ultrasound have been found to improve delivery to tumors, enhancing accumulation and penetration. We used a subcutaneous prostate cancer xenograft model in mice to investigate the effect of free and nanoparticle-encapsulated cabazitaxel in combination with ultrasound and microbubbles with a lipid shell or a shell of nanoparticles. Sonopermeation reduced tumor growth and prolonged survival (26%−100%), whether the free drug was co-injected with lipid-shelled microbubbles or the nanoformulation was co-injected with lipid-shelled or nanoparticle-shelled microbubbles. Coherently with the improved therapeutic response, we found enhanced uptake of nanoparticles directly after ultrasound treatment that lasted several weeks (2.3 × −15.8 × increase). Neither cavitation dose nor total accumulation of nanoparticles could explain the variation within treatment groups, emphasizing the need for a better understanding of the tumor biology and mechanisms involved in ultrasound-mediated treatment. (E-mail: sofie.snipstad@sintef.no)

Key Words: **Microbubbles, Drug delivery, Nanomedicine, Nanoparticles, Cabazitaxel, Ultrasound, Cavitation, Sonopermeation, Sonoporation, Sonochemotherapy.**

INTRODUCTION

Chemotherapy, alone or in combination with other treatment modalities, is one of the most common treatments for cancer patients (Chabner and Roberts 2005; Miller et al. 2019), but a lack of specificity combined with unfavorable pharmacokinetic properties limits the therapeutic benefit of the drugs. Only a small fraction of the dose reaches the target site (Kurdziel et al. 2011), and systemic toxicity limits the amount that can be administered. Several cytotoxic drugs have been encapsulated into nanoformulations with the aim of achieving more controlled delivery through passive targeting by the enhanced permeability and retention effect, triggered targeting or active targeting, and reduced side effects because of limited off-target accumulation (Lammers et al. 2012; Sanna et al. 2014). Nanocarriers may offer advantages such as improved control of pharmacokinetics and biodistribution, protection of the drug from premature interaction or degradation, improved cellular uptake, controlled and prolonged release profiles and combination therapies (Peer et al. 2007). Although many of the evaluated and approved nanoformulations have succeeded in reducing systemic toxicity, efficacy has only been improved in specific cases (Lammers et al. 2012; Anselmo and Mitragotri 2016; Petersen et al. 2016; Shi et al. 2017).

Small-molecule cytotoxic drugs and nanoparticles (NPs) are hindered by several biological barriers in the tumor microenvironment such as poorly perfused and necrotic regions, heterogeneous permeability of the vascular wall, high interstitial fluid pressure, a dense tumor stroma and extracellular matrix, cancer cell membranes and drug resistance (Lammers et al. 2012; Wilhelm et al. 2016). Recent findings suggest that active uptake through endothelial cells is more important than passive

Address correspondence to: Sofie Snipstad, Sem Sælands vei 2 A, 7034 Trondheim, Norway. E-mail: sofie.snipstad@sintef.no

uptake through the enhanced permeability and retention effect (Sindhwani et al. 2020) and that less than a percent of the injected dose of NPs is typically delivered to solid tumors (Wilhelm et al. 2016; Dai et al. 2018). One strategy increasingly applied to enhance local drug delivery is treatment of the tumor with ultrasound and microbubbles (MBs) to induce sonopermeation (Snipstad et al. 2018). The local oscillation of MBs caused by ultrasound can result in several bio-effects that enhance the permeability of the target tissue, allowing enhanced accumulation and improved penetration of the therapeutic agent. These effects have been explored in multiple preclinical studies (Lentacker et al. 2014; Liu et al. 2014; Lammertink et al. 2015; Boissenot et al. 2016; Van Wamel et al. 2016a, 2016b; Åslund et al. 2017a; Snipstad et al. 2017b; Lamsam et al. 2018; Meng et al. 2019) and in several published and ongoing clinical trials (ClinicalTrials.gov identifiers NCT04146441, NCT03458975, NCT03477019, NCT04021420, NCT03385200 and NCT04021277) (Kotopoulis et al. 2013; Carpentier et al. 2016; Dimcevski et al. 2016; Wang et al. 2018; Idbaih et al. 2019; Mainprize et al. 2019). Sonopermeation has been used to improve delivery and accumulation of a wide range of substances to solid tumors and across the blood–brain barrier, including chemotherapeutic drugs, neurotrophic factors, interleukins, antibodies, viral vectors and genes, NPs, stem cells and cells for immunotherapy (Snipstad et al. 2018). Various types of MBs are available for sonopermeation; however, all commercially available MBs were made and are approved for diagnostic purposes. Inclusion of NPs on the MB shell has been reported to make delivery of NPs more effective both *in vivo* (Burke et al. 2011, 2014) and *in vitro* (De Cock et al. 2016).

We have previously reported an in-house-made treatment platform consisting of protein MBs stabilized by polymeric NPs (NPMBs) containing the cytotoxic drug cabazitaxel and fluorescent dyes for imaging, coated with poly(ethylene glycol) (PEG) (Mørch et al. 2015). Cabazitaxel is an anti-microtubule agent that inhibits mitosis and promotes apoptosis. It is effective against cancers with resistance to other taxanes, and is approved for treatment of metastatic prostate cancer. The poly(alkyl cyanoacrylate) (PACA) NPs have been characterized with respect to cellular uptake, degradation and toxicity (Sulheim et al. 2016, 2017), surface PEGylation (Åslund et al. 2017b), stability of fluorescent payloads (Snipstad et al. 2014, 2017a), *in vivo* circulation time and biodistribution (Åslund et al. 2017b; Snipstad et al. 2017b) and efficacy (Fusser et al. 2019). NPMBs have also been used to enhance the delivery and therapeutic effect of NPs in solid tumors (Snipstad et al. 2017b; Yemane et al. 2019) and across the blood–brain barrier (Åslund et al. 2015; Baghirov et al. 2018; Sulheim et al. 2019). In our previous study (Snipstad et al. 2017b), we compared NPMBs used with and without ultrasound. In the present study, we aimed to investigate the effect of sonopermeation on delivery of free and NP-encapsulated cabazitaxel to solid tumors, and we hypothesized that sonopermeation would improve delivery of both formulations. We further aimed to compare the therapeutic effects of two different types of MBs: a co-injection of the two forms of cabazitaxel (clinically formulated and nanoformulated) with SonoVue, and nanoformulated cabazitaxel co-injected with in-house-made NPMBs with a shell of NPs. We hypothesized that the NPMBs would be more efficient because of the close proximity between MBs, NPs and tissue (De Cock et al. 2016). Based on previous experience with subgroups of responders and non-responders, we also aimed to evaluate if therapeutic response or variation within groups could be predicted by cavitation dose or measured tumor uptake of NPs. Furthermore, another tumor model was used, more control groups were included and the group sizes were increased compared with those in the previous efficacy study (Snipstad et al. 2017b).

METHODS

All chemicals were purchased from Sigma-Aldrich (St. Louis, MO, USA) unless otherwise specified.

Formulation of cabazitaxel, NPs and MBs

Cabazitaxel was administered either as the clinical formulation Jevtana or encapsulated in poly(2-ethylbutyl cyanoacrylate) (PEBCA) NPs. To make Jevtana, cabazitaxel (Biochempartner Co. Ltd, Wuhan, Hubei, China) was dissolved in distilled water with 1040 mg/mL polysorbate 80 (Tween 80) to 40 mg/mL and from there in 13% (w/w) ethanol to 10 mg/mL. Sodium chloride (0.9%) was then added before injection, resulting in a final concentration of 3 mg/mL.

To synthesize PEBCA NPs, a one-step mini-emulsion polymerization was performed as previously described (Mørch et al. 2015). Briefly, a water phase containing Brij L23 (7 mM, 23 PEG units, MW 1225) and Kolliphor HS15 (9 mM, 15 PEG units, MW 960) in 0.1 M HCl was mixed with an oil phase consisting of the monomer 2-ethyl butyl cyanoacrylate (Cuantum Medical, Bellaterra, Spain), 4 wt% Miglyol 812 (co-stabilizer, Cremer, Hamburg, Germany), 2.2 wt% vanillin, 10% w/v cabazitaxel, 0.12 wt% of the fluorescent dye NR668 (Klymchenko et al. 2012; Snipstad et al. 2017a) and 0.12 wt% of the near-infrared fluorescent dye IR780-lipid (Jacquart et al. 2013). The mixture was sonicated for 3 min on ice (50% amplitude, Branson Ultrasonics Digital Sonifier 450, Danbury, CT, USA). The solution was kept on rotation (15 rpm, SB3 rotator, Stuart, UK)

overnight at room temperature before adjusting the pH to 5 using 0.1 M NaOH. Polymerization was continued for 5 h at room temperature on rotation. The dispersion was dialyzed (Spectra/Por dialysis membrane MWCO 12-14000 Da, Spectrum Labs, Rancho Dominguez, CA, USA) against 1 mM HCl to remove unreacted PEG. Size, zeta potential and size distribution of the NPs were measured by dynamic light scattering (Zetasizer, Malvern Instruments, Malvern, UK). Drug loading was measured by extracting the drug from the particles by dissolving them in acetone at 1:10 NPs:acetone, before quantification by high-pressure liquid chromatography coupled to mass spectrometry (LC-MS/MS, Agilent 6490 triple quadrupole coupled with Agilent 1290 HPLC, Agilent Technologies, Santa Clara, CA, USA). Directly before injection into mice, the NPs were diluted in 0.9% sodium chloride to a concentration of 36.7 or 14.3 mg NP/mL.

NPMBs were made by mixing 0.75% w/v PEBCA NPs with casein (0.5% w/v) in 0.9% phosphate-buffered saline. The solution was saturated with perfluoropropane for 10 s (F2 Chemicals, Preston, UK) before being mixed with an Ultra Turrax (24,000 rpm, Branson Ultrasonics, Danbury, CT, USA) for 4 min. The resulting MBs were imaged in Countess cell counting chambers (ThermoFisher Scientific, Waltham, MA, USA) and analyzed in ImageJ (National Institutes of Health, Bethesda, MA, USA) (Schneider et al. 2012) to determine size and concentration. The resulting MB solution contains an excess of free NPs (approximately 99% of the NPs are free, the remainder are on MBs). On removal of free NPs from the solution, the NPMBs become less stable, which is why we decided to keep the remaining NPs in solution. To visualize the morphology of the NPMBs, they were sputter coated with 5-nm gold (Cressington 308 R, Cressington Scientific Instruments Ltd, Watford, UK) and imaged by scanning electron microscopy (SEM) using an S5500 S(T)EM (Hitachi High-Tech Corp., Tokyo, Japan).

SonoVue were prepared according to the supplier's (Bracco Imaging, Milan, Italy) recommendations. Five milliliters of sodium chloride 9 mg/mL (0.9%) solution was injected through the septum into the contents of the vial. The vial was then shaken vigorously for 30 s until the lyophilizate was completely dissolved. The MBs were imaged in Countess cell counting chambers (diluted 10 ×) and analyzed in ImageJ to determine size and concentration.

Cell culture

Prostate adenocarcinoma (PC3) cells (American Type Culture Collection, CRL-1435, Manassas, VA, USA) were cultured in Dulbecco's modified Eagle's medium (Gibco Invitrogen, Carlsbad, CA, USA) supplemented with 10% fetal bovine serum and 1% v/v penicillin−streptomycin (100 U/mL and 100 μg/mL). The cells were maintained in exponential growth at 37°C with 5% CO_2. Before tumor inoculation, the cells were detached by trypsinization, counted and resuspended in medium.

Animals and tumor xenografts

Female balb/c nude mice were purchased at 8 wk of age from Janvier Labs, France. They were housed in groups of six in individually ventilated cages in a specific pathogen-free environment at 22°C−23°C and 50%−60% relative humidity, on a 12 h light/dark cycle and with 70 air changes per hour and free access to food and sterile water. They were fed RM1 expanded pellets (Special Diets Services, Essex, UK), and the cages were enriched with housing, nesting material and gnaw sticks. During all experiments, the animals were anesthetized by inhalation of 2%−3% isoflurane (Baxter, Deerfield, IL, USA). Anesthesia was maintained with isoflurane in 0.4 L/min O_2 and 0.6 L/min N_2O during catheterization, imaging and general handling, and in 1.0 L/min medical air during the ultrasound treatments and ultrasound imaging to avoid reduced circulation time of the MBs (Mullin et al. 2011).

To establish subcutaneous tumor xenografts, 3×10^6 cells in 50 μL of medium were injected into the hind leg. The tumors were measured, and the animals weighed once or twice a week by a blinded researcher who did not know to which group the animals belonged. Tumor volume was calculated as $\pi l w^2/6$, where l is the length and w is the width of the tumor measured with calipers. A tail vein catheter (24 GA BD Neoflon, Becton, Dickinson, Franklin Lakes, NJ, USA) was placed for intravenous injection of drug and MBs. During implantation, treatment and imaging, the body temperature was maintained by placing the mouse on a heating pad or under a heating lamp, and the eyes were kept moist (Viscotears, Alcon, Geneva, Switzerland). When the tumors reached 15 mm in length, the animals were euthanized by cervical dislocation, and tumor and organs were excised. All experimental procedures were approved by the Norwegian Food Safety Authority.

MBs circulation time

The circulation time of MBs was investigated by comparing the pulsed wave (PW) Doppler signals from the carotid artery in mice using the Vevo3100 (Fujifilm Visualsonics, Toronto, Canada) and the MX550 D transducer at 32 MHz. The signal intensity of the PW Doppler spectrum increases when MBs are injected, and as they clear from circulation, the signal level returns back to baseline. A total of four mice were included, and each mouse received two injections of SonoVue and two injections of NPs+NPMBs, each of 50-μL given 10 min

apart. The carotid artery was located by scanning in B-mode, and the PW Doppler cursor was placed on the artery. The transducer was kept in a fixed position during the entire experiment, and the gain level was adjusted to a minimum, to avoid signal saturation as the MBs were injected. Data were recorded for 3−5 min after each injection. After the last injection, the mice were euthanized by cervical dislocation while in general anesthesia. The radiofrequency signal from the scanner was exported to MATLAB (R2019 a, The MathWorks Inc., Natick, MA, USA), and the linear signal intensities of all the pixels in the PW Doppler spectrum from each heartbeat were summed to give one data point on the time−intensity curve. The data were filtered to account for time variations caused by breathing and then normalized to compare the two bubble types. The heart rate of the animals was monitored during injections.

Ultrasound setup and treatment

For ultrasound treatment, the mouse was positioned on top of a water tank with the tumor-bearing leg lowered into the water through a 10-mm opening in the lid as described previously (Snipstad et al. 2017b) and seen in Figure 1. The surface of the lid was covered with an absorbing material to avoid standing waves (polyester wadding of 7-mm thickness). A custom-made single-element focused ultrasound transducer with a center frequency of 1 MHz was used (Imasonic SAS, Voray sur l'Ognon, France). The geometric focus of the transducer was at 12 cm, but to ensure that the entire tumor would be sonicated, the tumor-bearing leg was positioned at 19 cm, which is in the far field of the transducer. The transducer was calibrated in an Onda AIMS III water tank with an HGL-0200 hydrophone (Onda Corp., Sunnyvale, CA, USA), and the beam widths at 19 cm were found to be 6 and 10 mm at 3 and 6 dB, respectively. A waveform generator (33500 B, Keysight Technologies, Santa Rosa, CA, USA) and a 50-dB power amplifier (2100 L from Electronics and Innovations Ltd., Rochester, NY, USA) were used to generate ultrasound waves with a pulse length of 10 ms (10,000 cycles) and a peak negative pressure of 0.5 MPa (mechanical index = 0.5). A pulse repetition frequency of 0.25 Hz was applied (duty cycle of 0.25%), and the total treatment time was 15 min.

Passive cavitation detection was included using an unfocused 5-MHz transducer (V307-SU, Olympus, Tokyo, Japan) with an aperture of 2.54 cm, positioned in the corner of the water tank and pointed toward the immersed tumor-bearing leg, as illustrated in Figure 1. Each treatment consisted of 225 bursts, and the first millisecond of the acoustic signal from each burst was recorded at a sample rate of 100 MS/s by an oscilloscope (LeCroy Wavesurfer 44 Xs, Teledyne LeCroy, Chestnut Ridge, NY, USA) and transferred to a laptop for further analysis in MATLAB. The frequency content of the received signal was analyzed using Welch's overlapped averaging estimator with a moving Gaussian window with 50% overlap. A window size one-eighth of the total size of the recorded signal was chosen both to minimize the noise level and to preserve the frequency content. The cavitation dose per burst was defined as the mean broadband signal level in the frequency ranges between harmonic and superharmonic peaks in the frequency range from 1.5 to 5 MHz (*i.e.,* 1.6−1.9, 2.1−2.4, 2.6−2.9, 3.1−3.4, 3.6−3.9, 4.1−4.4 and 4.6−4.9 MHz). The cavitation dose for each burst transmitted during the 15 min of ultrasound treatment was found for each treatment and animal, and the standard deviation within treatment groups was calculated. The total cavitation dose for each treatment was found by summing the doses of individual bursts. Spectrograms of the recorded data from each treatment were calculated using a moving Gaussian window of 10,000 samples and 50% overlap.

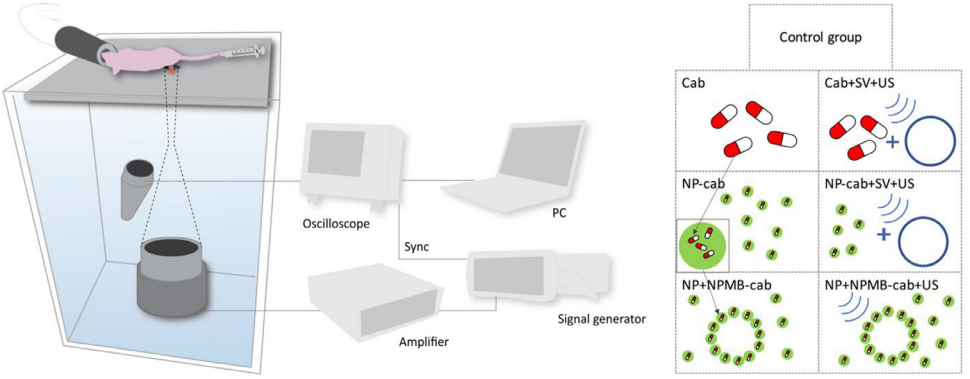

Fig. 1. Schematic of the ultrasound setup and graphic overview of the treatment groups included in the study. The ultrasound setup includes gas anesthesia for the animal, a water tank with the transducers for treatment and cavitation detection, as well as a signal generator, an amplifier and an oscilloscope connected to a computer. cab = cabazitaxel; NP = nanoparticles; US = ultrasound; SV = SonoVue; NPMB = microbubbles stabilized by NPs and protein.

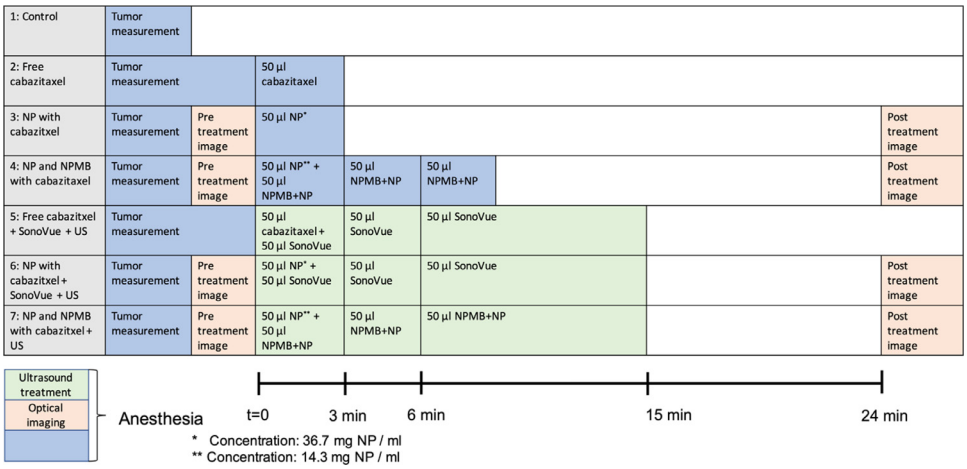

Fig. 2. Timeline and graphic representation of the groups. *Green shading* represents ultrasound treatment, *orange shading* represents near-infrared imaging and *blue shading* represents tumor size measurements or injections. NP = nanoparticles; NPMB = microbubbles stabilized by NPs and protein; US = ultrasound.

Whole-animal imaging and image analysis

The biodistribution and tumor uptake of NPs were measured using a near-infrared Pearl Impulse small imaging system (LI-COR Biosciences, Lincoln, NE, USA). Excitation and emission settings were 785 and 820 nm, respectively. The animals were imaged before and approximately 24 min after the first NP injection in weeks 1, 2 and 3 (approximately 9 min after the end of ultrasound treatment to give the NPs some time to extravasate). In addition, they were imaged in weeks 5 and 7. All images were processed in Fiji (ImageJ 1.51 c), and the mean fluorescence was quantified from regions of interest on the tumor-bearing leg and the healthy control leg on the opposite side. The researcher who performed the analysis was blinded and did not know which animals belonged to which groups. Regions of interest were also made on the abdominal and thoracic regions of the animal to quantify the amounts of NPs in the different organs for one selected time point.

Treatment groups and dosing

A total of 100 mice were included in this part of the study. They were randomly distributed into seven treatment groups:

1. Control (no treatment), n = 15
2. Free cabazitaxel (cab), n = 13
3. NPs with cabazitaxel (NP-cab), n = 14
4. NPs and NPMBs with cabazitaxel (NP + NPMB-cab), n = 16
5. Free cabazitaxel + Sonovue + ultrasound (cab + SV + US), n = 12
6. NPs with cabazitaxel + Sonovue + ultrasound (NP-cab + SV + US), n = 14
7. NPs and NPMBs with cabazitaxel + ultrasound (NP + NPMB-cab + US), n = 16

The treatment started 11 d after cell inoculation, when the mean tumor size was 59 ± 15 mm^3 (with a length of approximately 5–6 mm) and was repeated once a week for 3 consecutive wk. The animals in the control group (group 1) were anesthetized but received no treatment. The animals in groups 2–7 received a weekly dose of 0.15 mg cabazitaxel per mouse in different forms (7.5 mg/kg for a 20-g mouse, mean weight: 20.7 ± 1.1 g on inoculation day). Groups 3, 4, 6 and 7 received the same total dose of NPs, 1.84 mg PACA NPs per mouse; however, groups 4 and 7 received 61% of the NP dose as NPMB solution. A graphic representation of the various groups is provided in Figure 1, and the different treatment schemes and injection volumes are illustrated in Figure 2. For all groups to which MBs were administered (groups 4–7), the first MB bolus was administered directly after the injection of cabazitaxel or NPs, and the three MB boluses were given at 0, 3 and 6 min in the total 15-min ultrasound treatment. The same time points were also used for the groups that received MBs but no ultrasound. SonoVue was administered undiluted to administer approximately the same amount of MBs as for the groups treated with NPMBs.

Mice with tumors smaller than 200 mm^3 2 wk after the last treatment (day 29) were defined as partial responders, whereas mice with tumors smaller than 25 mm^3 at the end of the study (day 92) were defined as responders.

The effect of ultrasound and MBs alone without any drugs was studied in a separate experiment. Treatment started at day 18 with average tumor size of 98 ± 35 mm^3, and ultrasound treatment was given for 9 min

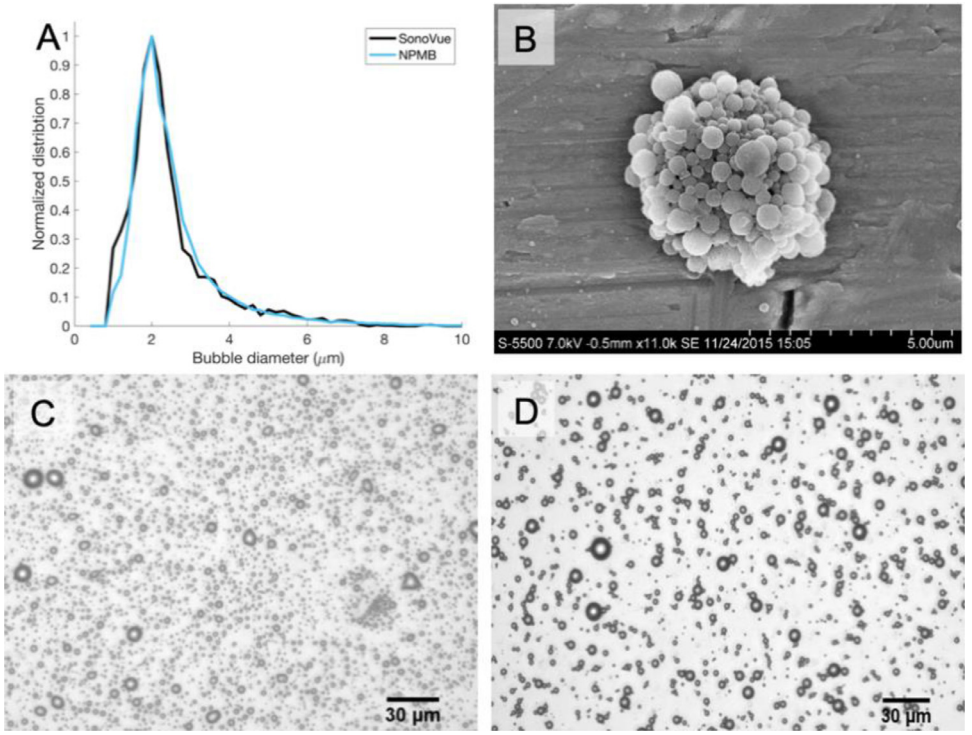

Fig. 3. Characterization of MBs. (a) Size distribution of SonoVue and NPMBs based on the analysis of 3 batches. (b) Scanning electron microscopy image of the NPMB. (c, d) Bright field microscopy images of NPMBs and (d) SonoVue. NP = nanoparticles; NPMB = microbubbles stabilized by NPs and protein; SV = SonoVue.

instead of 15 min. The mouse strain, tumor model and experimental design were otherwise the same as described above. To reduce the number of mice, ultrasound only was not included as the ultrasound exposure level is not expected to cause any bio-effects. A total of 31 animals were included and divided randomly into four groups:

1. Control (no treatment), n = 8
2. SonoVue and ultrasound (SV + US), n = 7
3. Empty NPs + NPMBs and ultrasound (NP + NPMB + US), n = 8
4. Free cabazitaxel (cab), n = 8

Statistical analysis

Statistical analysis was performed using R and Python. A significance level of 0.05 was used to assess statistical significance in all hypothesis tests. As it was of interest to compare the tumor growth of all seven groups at individual time points, multiple Shapiro–Wilk tests were conducted to test for normality. It was concluded that the data were not univariate normal for most time points and groups, especially at later time points. As the data were not normal, a non-parametric method, pairwise Wilcoxon rank sum tests, was performed to test for significance. To handle the problem of multiple comparisons, the false discovery rate was used to adjust the p values. The tumor growth analysis was performed with Stats (R Core Team 2017) package in R.

Survival was analyzed through Kaplan–Meier estimates using the log-rank test to check for significance. As it was of interest to compare groups, pairwise log-rank tests were performed using the Bonferroni correction. For each individual time point, only groups containing more than three mice were included in the hypothesis testing. The survival analysis was done using the Lifelines (Davidson-Pilon 2019) library in Python.

RESULTS

NPs and MBs

Cabazitaxel formulated as Jevtana formed micelles/clusters around 10 nm in size in aqueous solution (Sulheim et al. 2019). The average size of the cab-loaded NPs was 169 ± 94 nm, with a polydipersity index of 0.175, zeta potential of −3.2 ± 4.4 mV and drug loading of 8.2%. The average size of the NPMBs was 2.4 ± 1.3 μm, and the concentration was (6 ± 0.32) × 10^8 MBs/mL. The size distributions of the NPMBs and SonoVue are illustrated in Figure 3, along with a SEM image of the NPMBs and

microscopy images of NPMBs and SonoVue. SonoVue was found to have a size and concentration of 2.4 ± 0.4 μm and 3×10^8 MBs/mL, respectively, which correspond well to those reported previously (2.5 μm and $1-5 \times 10^8$ MBs/mL) (Schneider 1999).

Circulation time of MBs

Repeated injections of MBs in mice revealed that the average circulation half-lives of SonoVue and NPMBs were 27.5 ± 8.5 and 50.3 ± 18.1 s, respectively. At 180 s after the injection, the signal level was 15.4 ± 2.5% of the maximum for SonoVue and 20.6 ± 6.4% for NPMBs. Supplementary Figure S1 (online only) is a representative time−intensity plot. On the basis of the measured circulation time, the treatment schedule with three repeated injections at 0, 3 and 6 min was chosen. Shortly after the injection of NP + NPMB, a drop in the heart rate of 10%−40% lasting from 3−10 s was observed. Injection of SonoVue did not cause any change in the heart rate.

Tumor growth and survival

Tumor growth and survival for all the different groups are illustrated in Figures 4 and 5, respectively. There was a large variation in response within the various treatment groups, and the tumor growth curves for the individual tumors are provided in Figure 4b−d. The number of responders, as well as 50% survival and overall survival at the end of the study, are given in Table 1.

The untreated control group had the fastest tumor growth and, accordingly, the shortest survival. All groups treated with cabazitaxel responded to treatment with reduced tumor growth, and all groups except NP + NPMB-cab significantly differed from untreated controls from days 7 to 29 (at which point most controls had been euthanized; all p values can be found in Supplementary Table S1, online only).

Tumors treated with free cabazitaxel responded somewhat better than those treated with encapsulated cabazitaxel (NP-cab), with a higher number of

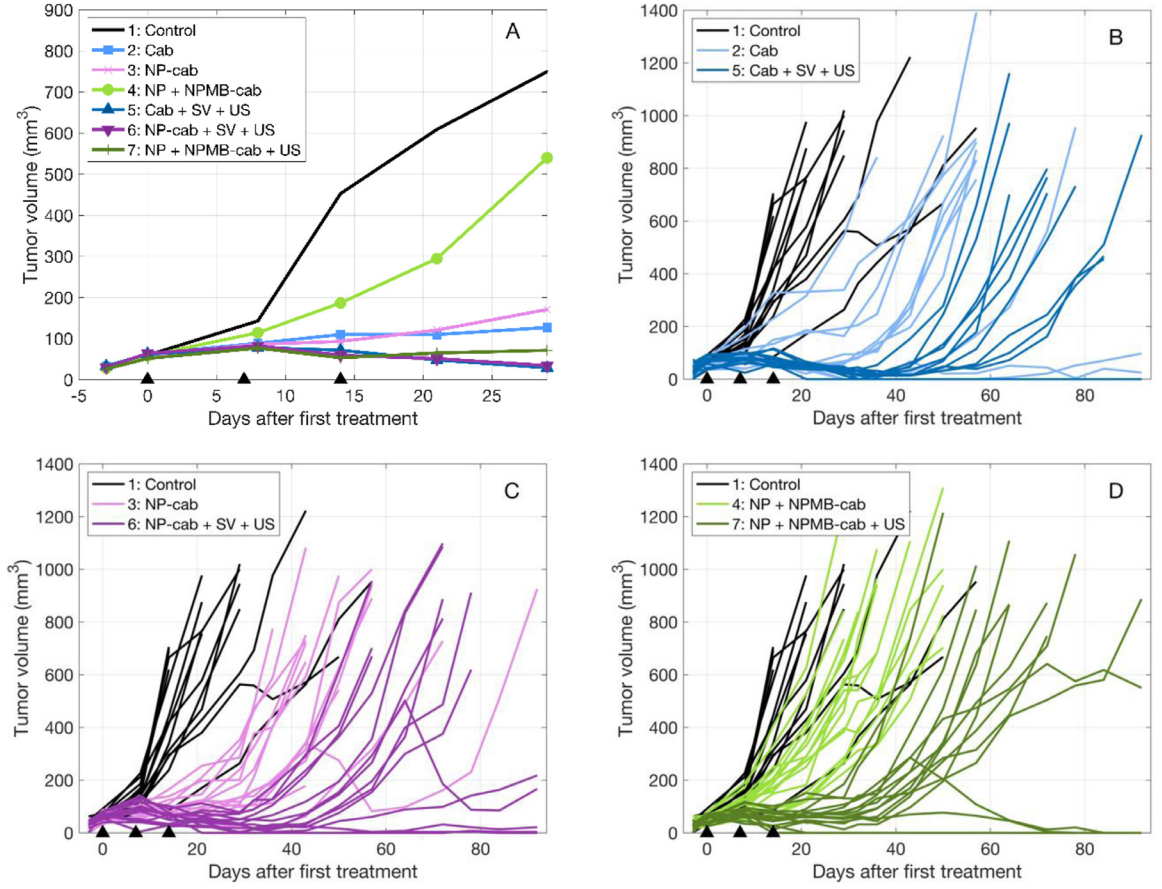

Fig. 4. Tumor growth with time. (a) Tumor growth for the seven different groups until day 29. Data points are group means, and treatments were performed on days 0, 7 and 14 (marked with *black triangles*). Standard deviations are not shown for improved readability, but tumor growth for all individual animals until the end of the study is shown in (b)−(d). All animals represented by dark colors (*blue/pink/green*) were treated with ultrasound and MBs, and those represented by lighter colors were given only the drug (free or encapsulated in NP/NPMB). Untreated control animals are represented by *black lines*. cab = cabazitaxel; NP = nanoparticles; NPMB = microbubbles stabilized by NPs and protein; SV = SonoVue; US = ultrasound.

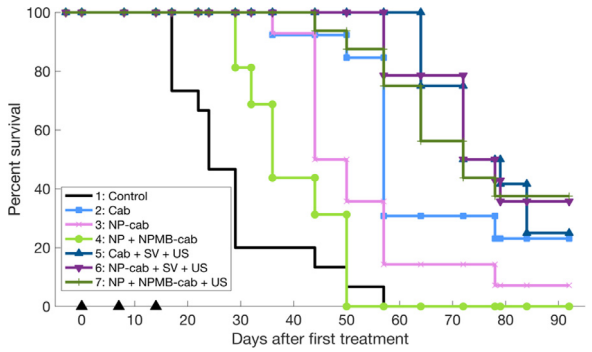

Fig. 5. Kaplan–Meier survival plot for the seven different groups. Treatments were performed on days 0, 7 and 14 (marked with *black triangles*). Animals that reached the endpoint with respect to tumor size were euthanized at various times from day 17 to the end of the study at day 92. cab = cabazitaxel; NP = nanoparticles; NPMB = microbubbles stabilized by NPs and protein; SV = SonoVue; US = ultrasound.

responders, but the difference in tumor growth was not significant.

Sonopermeation enhanced the therapeutic effect for all groups. The most significant effect of ultrasound and MBs was seen when comparing the groups given NP + NPMB with and without ultrasound. The tumor growth in the NP + NPMB-cab + US group was significantly lower than that in the NP + NPMB-cab group from day 7 and onward, while median survival increased by 100%. The NP-cab + SV + US group had significantly lower tumor growth than the NP-cab group from day 14 onward, while the median survival increased by 64%. The cab + SV + US group only had significantly lower tumor growth than the cab group in a brief period after the treatment, but there was no significant difference during the last 40 d of the follow-up period. However, the added sonopermeation resulted in an increase in median survival by 26%. The Kaplan–Meier plot illustrates that survival of the NP + NPMB-cab + US group was significantly longer than that of the NP + NPMB-cab group (p value: 2.53×10^{-7}), and the survival of the NP-cab + SV + US group was longer than that of the NP-cab group (p value: 1.37×10^{-4}), but cab + SV + US did not significantly differ from cab (p value: 0.317) (Kaplan–Meier curves with 95% confidence intervals are illustrated in Supplementary Fig. S2 [online only]).

When the three different ultrasound treated groups were compared, the Wilcoxon test revealed that the cab + SV + US group had significantly lower tumor growth for a period (day 29 to 50), but from day 57 onward, no significant differences between the different types of MBs were observed, and the median survival was similar for all three groups treated with ultrasound and MBs.

Tumor growth of animals that were treated with SonoVue or NPMBs in combination with ultrasound but without any drug was similar to that of the untreated controls (Supplementary Fig. S3, online only).

Imaging NPs accumulation

Whole-animal imaging revealed that sonopermeation clearly enhanced the uptake of NPs in the treated tumor leg for both the NP-cab + SV + US and NP + NPMB-cab + US groups compared with animals that did not receive ultrasound treatment (NP-cab and NP + NPMB-cab groups). Representative images are provided in Figure 6, where the animals are imaged in the dorsal position and the tumor is on the left hindleg. Mean fluorescence values from regions of interest on the tumor-bearing leg and the control leg on the opposite side are illustrated in Figure 6b and 6c. In the ultrasound-treated tumors, the accumulation of NPs appears to continue to increase until the pre-image in the next week. The absolute values exhibit increased uptake from pre- to post-images for each week in the ultrasound-treated tumors. Sonopermeation increased tumor uptake by $2.3\times - 15.8\times$ compared with the tumor uptake in the corresponding control groups without ultrasound, as illustrated in Figure 6d. To obtain insight into why some animals respond better to the treatment than others, the uptake of NPs was correlated to the tumor growth within each group. The variation in therapeutic response within each group could not be explained by a difference in uptake of NPs in these images. Uptake of NPs in the thoracic and abdominal regions is illustrated in Supplementary Figure S4 (online only). The NP-cab group exhibited significantly increased accumulation in the lungs (thoracic region) compared with the other groups. The NP-cab, NP-cab + SV + US and NP + NPMB-cab + US groups all had similar accumulation in the liver–kidney–spleen region (abdominal region), whereas the NP + NPMB-cab group had significantly less accumulation than the NP + NPMB-cab + US group.

Cavitation detection

During the ultrasound treatment, the acoustic signal from the MBs circulating in the tumor-bearing leg was detected by a separate passive receive transducer. The circulating bubbles caused increased signal at sub- and superharmonics and a general increase in the broadband level. An example of the frequency content of the received signal from a burst transmitted before and after an injection of SonoVue is illustrated in Figure 7a. The combination of a general broadband noise level increase and peaks at the subharmonic (0.5 MHz) and superharmonic (1.5, 2.5, 3.5 MHz, *etc.*) indicated that there may have been a combination of inertial and stable cavitation. The spectrograms in Supplementary Figure S5 (online

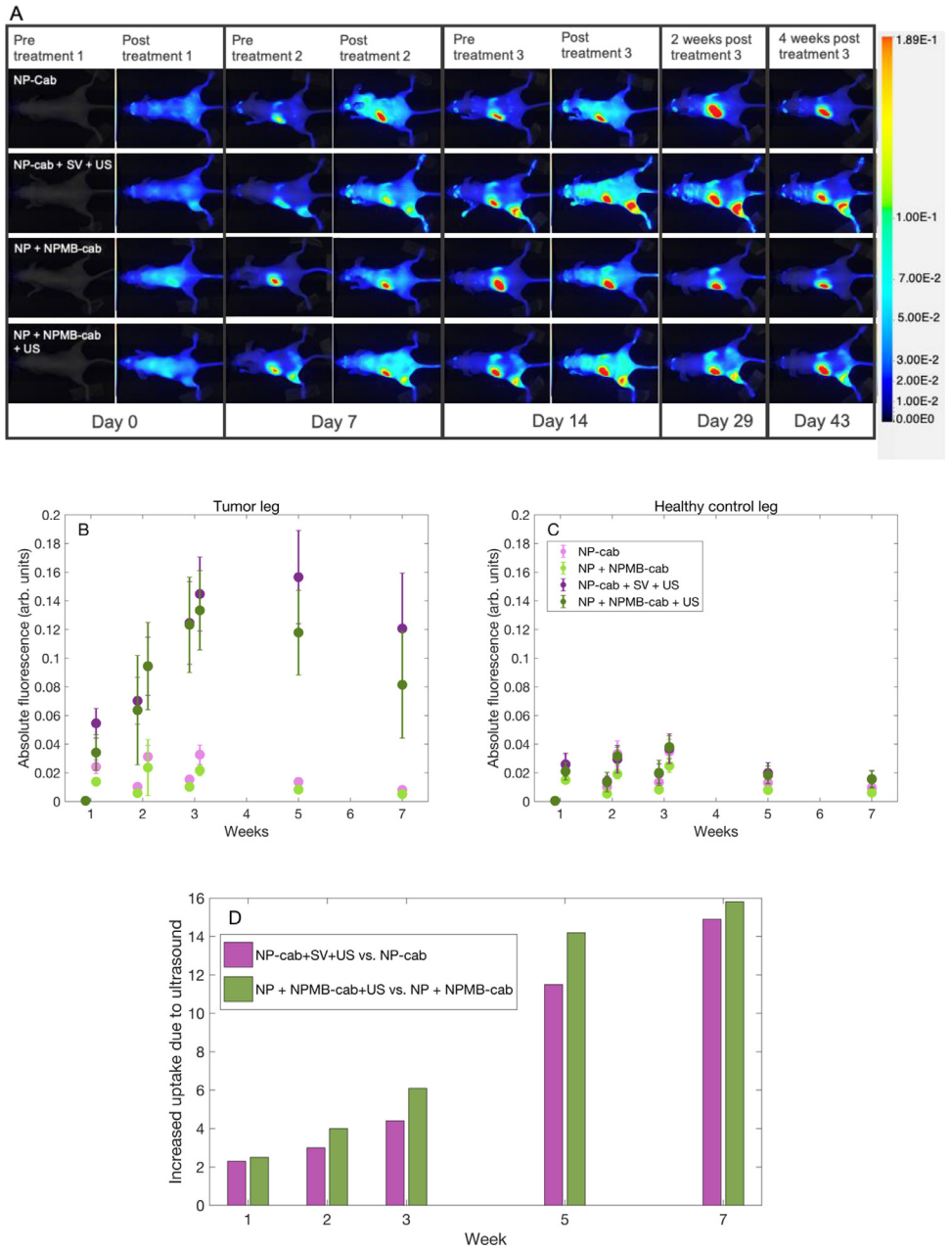

Fig. 6. Biodistribution and tumor uptake of NPs. (a) Representative images illustrating *in vivo* biodistribution in an animal from each of the groups given NP-cab with and without SonoVue and US (first and second rows) and NP + NPMB-cab with and without US (third and fourth rows). The tumor is on the left hindleg. From left to right are pre- and post-images for the first, second and third treatments and images 2 and 4 wk after the last treatment. The color bar represents arbitrary fluorescence units. (b, c) Uptake of NPs quantified as absolute fluorescence from tumor leg (b) and healthy control leg (c) for all NP- and NP + NPMB-treated groups. Treatments and imaging occurred in weeks 1–3, and the animals were also imaged in weeks 5 and 7. Pre- and post-data are on the left and right sides of the vertical line at each time point, respectively. Data points indicate group means with standard deviations; each group contains n = 14–16 animals. (d) Increased uptake of NPs caused by sonopermeation, shown as ratios of mean tumor uptake in NP-cab + SV + US group versus NP-cab group and NP + NPMB-cab + US-group versus NP + NPMB-cab group from post-treatment images. cab = cabazitaxel; NP = nanoparticles; NPMB = microbubbles stabilized by NPs and protein; US = ultrasound; SV = SonoVue.

only) contain examples of the frequency content as a function of time from treatments with NPMBs and SonoVue in combination with NP or cab. When the broadband signal levels from treatments with SonoVue and NPMBs are compared as a function of time, we see that SonoVue is cleared from the sonicated area during

Table 1. Total number of mice and number of partial responders (tumor volume <200 mm^3 2 wk after treatment) and responders (tumor volume <25 mm^3 at the end of the study), in addition to 50% and overall survival relative to the start of treatment

Group	Total No. of mice	50% survival (d)	Overall survival	Partial responders (tumor volume <200 mm^3 2 wk after last treatment)	Responders (tumor volume <25 mm^3 at end of study)
1. Control	15	24	0%	0%	0%
2. Cabazitaxel	13	57	23%	85%	15%
3. NP-cab	14	44	7%	64%	0%
4. NP + NPMB-cab	16	36	0%	0%	0%
5. Cabazitaxel + SonoVue + US	12	72	25%	100%	17%
6. NP-cab + SonoVue + US	14	72	36 %	100%	21%
7. NP + NPMB-cab + US	16	72	38 %	100%	25%

cab = cabazitaxel; NP = nanoparticles; NPMB = microbubbles stabilized by NPs and protein; US = ultrasound.

the 3 min between the injections and that the signal increases abruptly at the next injection (Fig. 7b–d). The signal from the NPMBs, however, is stable and even increases between injections, and the bubble signal decreases during the 6–9 min after the last injection (Fig. 7b–d). The signal level after the second and third bubble injections increases compared with that after the first injection for all three groups. Both groups treated with SonoVue have similar signal profiles as a function of time; however, the group receiving NP with encapsulated cabazitaxel has a consistently higher signal level from the MBs than the group receiving cabazitaxel in free formulation, even though the amount and type of MBs are the same. No correlation between cavitation dose and treatment response was found.

When the total cavitation doses received during the 15 min of ultrasound treatment (225 bursts) for the three groups were compared, it is apparent that NPMBs result in a higher cavitation dose compared with SonoVue for all treatments, as illustrated in Figure 7e. The total cavitation dose decreases slightly from the first to the second treatment but increases in the third.

Weight of mice and organs

To evaluate if any of the treatments caused toxicity in the animals or specific organs, weight was monitored weekly throughout the study, and all organs were excised and weighed when the animals were euthanized. Animal weights, illustrated in Supplementary Figure S6 (online only), anever decreased below the starting weight in any of the groups. Weights of liver, spleen, lungs, heart and kidneys for each individual animal for all groups are illustrated in Supplementary Figure S7 (online only). No significant differences were observed between the different organs in the different groups. Although this indicates that there were no severe long-term effects of the treatment, safety cannot be concluded because the organs might have recovered such a long time after treatment, and readouts other than weight would be more important for assessing organ-specific toxicity.

DISCUSSION

Sonopermeation increased the therapeutic efficacy of the various formulations of cabazitaxel. This was supported by the observed enhanced accumulation of NPs in the tumors compared with that in the tumors not treated with ultrasound. The observed increase caused by ultrasound treatment also corresponds well with our previous results (Snipstad et al. 2017b), and is likely owing to improved permeability of the tumor vasculature and enhanced penetration into extracellular matrix (Yemane et al. 2019). Tumor growth was similar for the three groups treated with ultrasound and MBs, indicating that the delivery was equally effective despite different formulations of the drug (free vs. encapsulated) and type of MB. It also indicates that the encapsulation of drug into NPs did not limit the efficacy of the drug. Treatment with ultrasound and MBs alone without drug did not affect tumor growth compared with that of untreated controls, indicating that the mechanical effect of the MBs by itself was not enough to induce any therapeutic effect. The similar response to the two types of MBs could be owing to the large surplus of NPs in the NPMB solution, and contrasts with what was observed for NP-coated MBs by Burke et al. (2011, 2014) and De Cock et al. (2016), who observed increased efficacy when NPs are attached to the MBs.

Even though the therapeutic responses to the different types of MBs were similar, the MBs exhibited different cavitation signals. A higher total cavitation dose indicates a higher number of cavitation events within the tissue that is exposed to ultrasound. An assumption within the field of ultrasound-enhanced drug delivery is that cavitation activity is the core of the delivery process. Hence, improved treatment efficacy would be expected for the NP + NPMB + US group. However, that is not the case for the experiments described here. The higher cavitation dose that was observed for NPMBs compared with SonoVue could be owing to the longer circulation time. From experiments in which MBs were imaged with PW

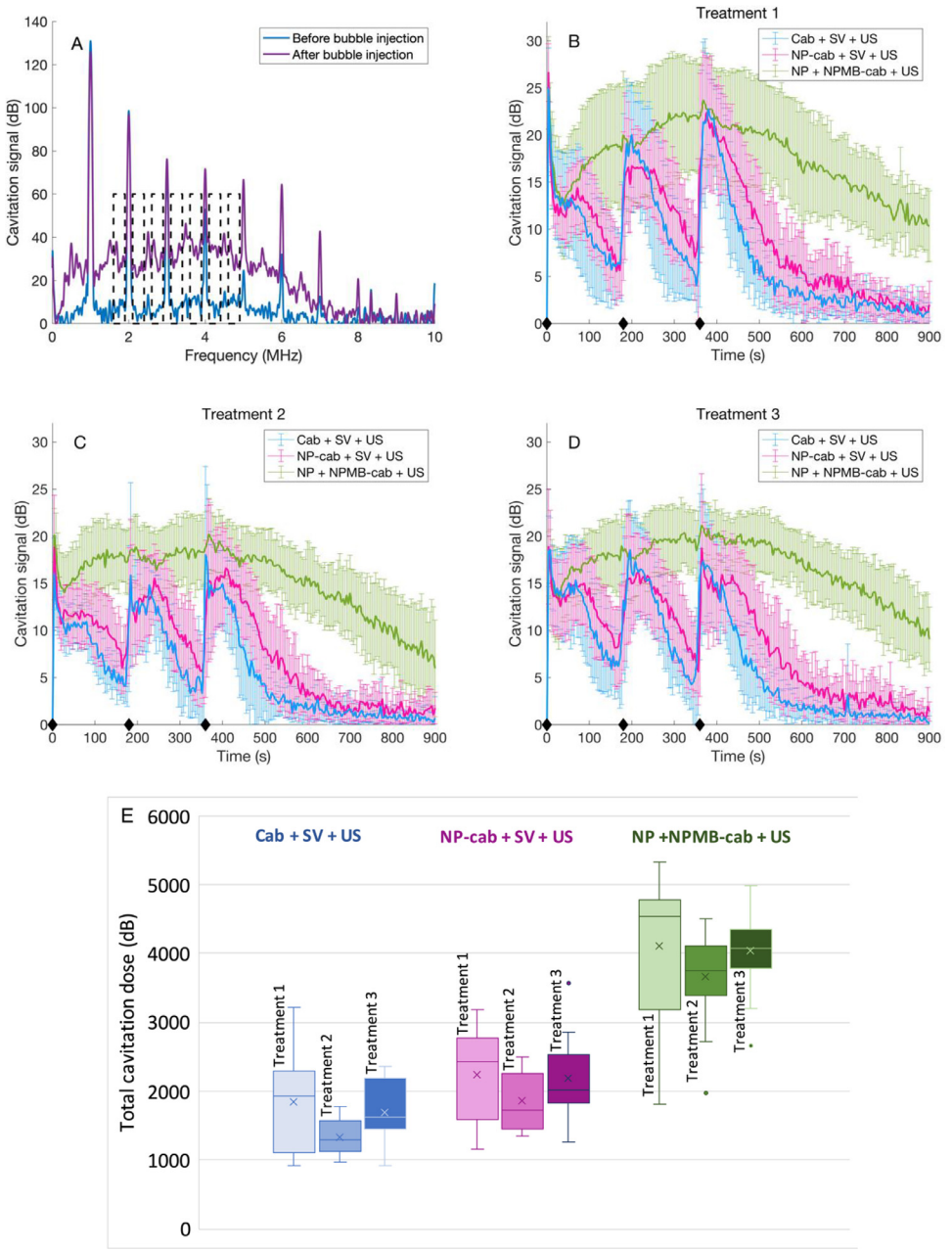

Fig. 7. Cavitation detection. (a) Example of the frequency content of the acoustic signal detected from the tumor-bearing leg from a burst given before (*blue*) and directly after (*purple*) a SonoVue injection. The signal level is relative to the general noise level of the oscilloscope. The *dashed black lines* mark the frequency range where the broadband cavitation signal is extracted. (b−d) Mean broadband cavitation signal and standard deviation from MBs circulating in the tumor-bearing leg during sonication of NPMBs (*green*) and SonoVue (*pink* and *blue*) in all animals during treatments 1−3. The animals received three injections, each containing 50 μL of MBs, at 0, 180 and 360 s, marked with *diamond symbols*. The tumor was sonicated for 15 min (900 s) with bursts lasting 10 ms transmitted every 4 s. (e) Total cavitation dose for each treatment (each including 225 bursts) in the three groups that were treated with ultrasound shown as a boxplot. Each box shows the median as a line, mean value as an x and second and third quartiles as lower and upper boundaries of the box. NP = nanoparticles; US = ultrasound; NPMB = microbubbles stabilized by NPs and protein.

Doppler techniques in the carotid artery of mice, we observed that NPMBs have a circulation half-life approximately 1.8 times that of SonoVue. Differences in diffusion of gas out of the MBs and clearance of the MBs by the reticuloendoethelial system could contribute to the differences in circulation half-life. The size distributions

of SonoVue and NPMBs are quite similar, but the shell properties, such as thickness and stiffness, are presumably different. SonoVue, having a thin and flexible lipid shell, will probably respond differently than NPMBs, which are more rigid and irregular, and the shell properties may vary more within the NPMB batch than for SonoVue. NPMBs were confirmed to be stiffer than SonoVue in attenuation measurements (Supplementary Fig. S8, online only). With a mechanical index of 0.5 and burst lengths of 10,000 cycles (10 ms), it was expected that all the MBs within the ultrasound field would be destroyed during a single burst; however, there may be a subpopulation within the NPMB batch that tolerated the acoustic pressures and persisted within the sonication field. This could explain the prolonged period of high-level cavitation signal from the NPMB injections. The increase in cavitation dose from bubble injection 1 to 2 and 3 could be caused by changes induced in vasculature or tumor perfusion, resulting in greater inflow of MBs, as observed by Rix et al. (2014) after contrast-enhanced ultrasound imaging. It could also be caused by stationary, stable MBs in the capillaries, which could be sticking to the capillary walls. An increased heart rate and peripheral vasodilation could possibly also explain the increased cavitation signal, counteracting the expected signal drop directly after injection. However, the heart rate was stable after SonoVue injections, whereas after injections of NPMBs, the heart rate frequently dropped. This temporary reduction of heart rate might affect peripheral blood flow and, thus, the amount of MBs producing cavitation signal. The decreased cavitation activity in week 2 and subsequent increase in week 3 could also be owing to more long-term changes in tumor perfusion caused by vasoconstriction, vascular shutdown or decompression, which have also been reported previously by others (Wood et al. 2005; Raymond et al. 2007; Goertz et al. 2012; Hu et al. 2012; Belcik et al. 2015; Keravnou et al. 2016; El Kaffas et al. 2018; Rix et al. 2019).

No correlation between tumor size and cavitation signal was found. One could expect an increased signal from larger tumors because there are more vessels in the field, but this was not the case. Even in mice in which the tumor was no longer detectable during the third treatment, we saw a cavitation signal similar to those for tumor volumes around $7 \times 5 \times 5$ mm^3. This could indicate that the setup used for cavitation detection was not sensitive enough to differentiate responders and non-responders, which was also the case for the setup used by Bazan-Peregrino et al. (2013), who did not find a correlation between uptake and cavitation. With the single-element transducer that was used, the recorded signal comes from the tumor-bearing leg as a whole, and it is possible that signal from large feeding arteries, arterioles and vessels in the skin dominates the signal from the capillaries in the tumor. One possible future extension could be passive cavitation mapping (Gyongy and Coussios 2010; Coviello et al. 2017) to image in real time where in the tumor the cavitation activity is.

Comparison of the three ultrasound-treated groups with their respective controls that did not receive ultrasound revealed that the largest effect of ultrasound was that for the NPMBs. Injecting only NP + NPMB had little effect on tumor growth, but the NP + NPMB combined with ultrasound performed equally well as the two other ultrasound-treated groups. One explanation for why the NP+NPMB group had faster tumor growth than the NP group (even though the majority of NPs in the NPMB solution are free and not bound to NPMBs) could be that some of the NPMBs (and/or NPs in the NPMB solution) end up in the lungs or other organs and that a smaller percentage of the cabazitaxel dose reaches the tumor compared with other groups. This could occur if the added casein caused aggregation of NPs or NPMBs in blood, leading to accumulation in the lungs, which is the first capillary network encountered after intravenous administration. However, this was not supported by the biodistribution of the NPs seen in whole-animal images. Other possible reasons the NP + NPMB group exhibited faster tumor growth than the group treated with NPs could be that the NPs in the NPMB solution are covered with casein and therefore removed from the circulation faster than NPs injected alone, or that the added casein causes the NPs to increase in size, aggregate more or become stickier and therefore extravasate/penetrate less efficiently in the tumor.

Free cabazitaxel was somewhat more efficient than the encapsulated cabazitaxel (NP-cab) in terms of the larger number of survivors, although the difference in tumor growth was not significant. This contrasts with the previously observed efficacy for the same type of NPs in a breast cancer model (Fusser et al. 2019), where the NP-cab group performed better than the free cab group. This difference is likely owing to differences in the microenvironments of the two tumor models. With sonopermeation, however, the NP-cab and the free cab groups performed fairly similarly (even slightly higher overall survival in the NP-cab group than the cab group), suggesting that the improvement resulting from ultrasound is more pronounced for the encapsulated formulation—likely because the accumulation and penetration through the extracellular matrix are more limited for the NPs compared with the free drug.

We used a subcutaneous prostate cell line-derived xenograft tumor model in immunocompromised mice, a model for which translatability might be limited. Female mice were used for convenience and consistency because

they were used in multiple previous studies by our group in which various tumor types were compared. Subcutaneous tumors will grow in both sexes; however, in future studies male mice would be preferred for the prostate xenografts. Another possible extension for future work is orthotopic tumor models, either of human origin in immunocompromised mice or of murine origin in immunocompetent mice. The latter would also enable investigation of effects on the (systemic) immune system. Such models might be physiologically more relevant to and more predictive of the clinical situation.

The cause of the short-term drop in heart rate after injection of NP + NPMB is unknown and requires further investigation, but could be linked to previous observations of reduced heart rate and transient apnea in the TRAMP (transgenic adenocarcinoma of the mouse prostate) model (Fagerland et al. 2020) or to the acute respiratory distress syndrome that was observed in patients treated with a polymeric nanoformulation of doxorubicin in a phase II clinical trial (Merle et al. 2017). No adverse long-term effects on the animals were observed in response to the additional sonopermeation treatment, suggesting that this is a tolerable and promising method to enhance the delivery and therapeutic effect of various drugs.

The fluorescent signal from NPs in tumors was visible for several weeks, indicating that the NPs could work as a sustained release system potentially releasing cabazitaxel for a prolonged time. This could be highly beneficial for drug delivery purposes compared with a bolus injection of a free drug that is rapidly eliminated. However, the NPs might degrade within this time, and the release profile of IR-780 lipid dye might differ from that of the encapsulated drug. Furthermore, the tumor accumulation 24 min after treatment (post-images) included NPs still in circulation, which can keep extravasating for the next hours, explaining the increased accumulation seen from one treatment to the next. This indicates that sonopermeation affects the tumor tissue both directly after treatment and over a prolonged period as the accumulation in tumor tissue increased with time during the treatment period.

One of the aims of the study was to investigate if there was a correlation between the amount of NPs accumulated in the tumor tissue or the cavitation dose and therapeutic efficacy. If so, those parameters could be used to predict which animals would respond well to the therapy. There was a clear indication that sonopermeation improved therapeutic efficacy, but the variation in response within groups could not be explained by the individual variations in NP uptake nor by the variation in cavitation dose. Other reasons for the subgroups of responders and non-responders could be individual differences in tumor microenvironment, for example, varying amount and structure of vasculature or connective tissue, differences in drug penetration into the extracellular matrix, clones of more or less responsive tumor cells caused by genetic diversity or differences in type or amount of residential or infiltrating immune cells (even though the balb/c nude mice lack T cells, they still have other types of immune cells that could affect tumor growth) (Wu et al. 2018). This emphasizes the importance of understanding tumor biology and the characteristic traits of a tumor that make it susceptible to such treatments, as well as the need to understand the mechanisms underlying sonopermeation to tune and optimize the technology. An increased understanding will help us to answer one of the important questions for future clinical application of ultrasound-mediated —drug delivery; how we can stratify patients by some form of imaging or screening of genetic or molecular markers to treat only the subset of patients that are likely to respond well to such treatment.

CONCLUSIONS

Sonopermeation enhanced the uptake of NPs and resulted in reduced tumor growth. No significant differences in therapeutic effect were observed between the three different ultrasound-treated groups, indicating that the three formulations—free drug combined with SonoVue, NPs with drug combined with SonoVue and NPs with drug combined with NPMBs—were equally effective. This indicates that sonopermeation can be used for different therapeutic formulations, both free molecular and encapsulated, with different types of MBs. The large variation within groups of responders and non-responders emphasizes the need for improved understanding of tumor biology and underlying mechanisms of sonopermeation in drug delivery.

Acknowledgments—Anne Rein Hatletveit, Maria Gellein and Kai Vernstad are acknowledged for technical support. The Comparative Medicine Core Facility (CoMed) at NTNU provided housing and care of animals and equipment for whole-animal imaging. Ida Marie Høiaas and Ida Sofie Jorstad are acknowledged for providing SEM images; SEM imaging was performed at NTNU NanoLab. The Research Council of Norway is acknowledged for their support of the Norwegian Micro- and Nano-Fabrication Facility, NorFab (Project No. 245963/F50).

The mechanical workshop at NTNU is acknowledged for building the water tank in the ultrasound setup, and Marikken Høiseth is acknowledged for illustrating the setup. The project was funded by the Research Council of Norway (240410/F20 Multibubble and 254832/O70 BubbleCAN, 296456/O30 BubbleCAN Milestone) and the Central Norway Regional Health Authorities.

Conflict of interest disclosure—S.S., Y.M., E.S., A.Å., C.D., R.H. and S.B. are co-inventors of a patent describing the nanoparticle-stabilized microbubbles (US20200023073 A1).

SUPPLEMENTARY MATERIALS

Supplementary material associated with this article can be found in the online version at doi:10.1016/j.ultrasmedbio.2020.12.026.

REFERENCES

Anselmo AC, Mitragotri S. Nanoparticles in the clinic. Bioeng Transl Med 2016;1:10–29.

Åslund AKO, Berg S, Hak S, Mørch Ý, Torp SH, Sandvig A, Widerøe M, Hansen R, Davies CdL. Nanoparticle delivery to the brain—By focused ultrasound and self-assembled nanoparticle-stabilized microbubbles. J Control Release 2015;220:287–294.

Åslund A, Snipstad S, Healey A, Kvåle S, Torp SH, Sontum PC, de Lange Davies C, van Wamel A. Efficient enhancement of blood−-brain barrier permeability using acoustic cluster therapy (ACT). Theranostics 2017a;7:23–30.

Åslund AKO, Sulheim E, Snipstad S, von Haartman E, Baghirov H, Starr N, Kvale Lovmo M, Lelu S, Scurr D, Davies CL, Schmid R, Morch Y. Quantification and qualitative effects of different PEGylations on poly(butyl cyanoacrylate) nanoparticles. Mol Pharm 2017b;14:2560–2569.

Baghirov H, Snipstad S, Sulheim E, Berg S, Hansen R, Thorsen F, Morch Y, Davies CL, Aslund AKO. Ultrasound-mediated delivery and distribution of polymeric nanoparticles in the normal brain parenchyma of a metastatic brain tumour model. PLoS One 2018;13 e0191102.

Bazan-Peregrino M, Rifai B, Carlisle RC, Choi J, Arvanitis CD, Seymour LW, Coussios CC. Cavitation-enhanced delivery of a replicating oncolytic adenovirus to tumors using focused ultrasound. J Control Release 2013;169:40–47.

Belcik JT, Mott BH, Xie A, Zhao Y, Kim S, Lindner NJ, Ammi A, Linden JM, Lindner JR. Augmentation of limb perfusion and reversal of tissue ischemia produced by ultrasound-mediated microbubble cavitation. Circ Cardiovasc Imaging 2015;8 e002979.

Boissenot T, Bordat A, Fattal E, Tsapis N. Ultrasound-triggered drug delivery for cancer treatment using drug delivery systems: From theoretical considerations to practical applications. J Control Release 2016;241:144–163.

Burke CW, Hsiang YH, Alexander Et, Kilbanov AL, Price RJ. Covalently linking poly(lactic-co-glycolic acid) nanoparticles to microbubbles before intravenous injection improves their ultrasound-targeted delivery to skeletal muscle. Small 2011;7:1227–1235.

Burke CW, Alexander Et, Timbie K, Kilbanov AL, Price RJ. Ultrasound-activated agents comprised of 5-FU-bearing nanoparticles bonded to microbubbles inhibit solid tumor growth and improve survival. Mol Ther 2014;22:321–328.

Carpentier A, Canney M, Vignot A, Reina V, Beccaria K, Horodyckid C, Karachi C, Leclercq D, Lafon C, Chapelon JY, Capelle L, Cornu P, Sanson M, Hoang-Xuan K, Delattre JY, Idbaih A. Clinical trial of blood-brain barrier disruption by pulsed ultrasound. Sci Transl Med 2016;8 343.re2.

Chabner BA, Roberts TG, Jr. Timeline: Chemotherapy and the war on cancer. Nat Rev Cancer 2005;5:65–72.

Coviello C, Myers R, Jackson E. Cavitation enhanced drug delivery in-vivo using combined B-mode guidance and real-time passive acoustic mapping: Challenges and results. J Acoust Soc Am 2017;141:3491.

Dai Q, Wilhelm S, Ding D, Syed AM, Sindhwani S, Zhang Y, Chen YY, MacMillan P, Chan WCW. Quantifying the ligand-coated nanoparticle delivery to cancer cells in solid tumors. ACS Nano 2018;12:8423–8435.

Davidson-Pilon C. Lifelines: Survival analysis in Python. J Open Source Softw 2019;4. doi: 10.21105/joss.01317.

De Cock I, Lajoinie G, Versluis M, De Smedt SC, Lentacker I. Sonoprinting and the importance of microbubble loading for the ultrasound mediated cellular delivery of nanoparticles. Biomaterials 2016;83:294–307.

Dimcevski G, Kotopoulis S, Bjånes T, Hoem D, Schjøtt J, Gjertsen BT, Biermann M, Molven A, Sorbye H, McCormack E, Postema M, Gilja OH. A human clinical trial using ultrasound and microbubbles to enhance gemcitabine treatment of inoperable pancreatic cancer. J Control Release 2016;243:172–181.

El Kaffas A, Gangeh MJ, Farhat G, Tran WT, Hashim A, Giles A, Czarnota GJ. Tumour vascular shutdown and cell death following ultrasound-microbubble enhanced radiation therapy. Theranostics 2018;8:314–327.

Fagerland SM, Berg S, Hill D, Snipstad S, Sulheim E, Hyldbakk A, Kim J, de Lange Davies C. Ultrasound mediated delivery of chemotherapy in the transgenic adenocarcinoma of the mouse prostate model. Ultrasound Med Biol 2020;46:3032–3045.

Fusser M, Overbye A, Pandya AD, Morch Y, Borgos SE, Kildal W, Snipstad S, Sulheim E, Fleten KG, Askautrud HA, Engebraaten O, Flatmark K, Iversen TG, Sandvig K, Skotland T, Maelandsmo GM. Cabazitaxel-loaded poly(2-ethylbutyl cyanoacrylate) nanoparticles improve treatment efficacy in a patient derived breast cancer xenograft. J Control Release 2019;293:183–192.

Goertz DE, Todorova M, Mortazavi O, Agache V, Chen B, Karshafian R, Hynynen K. Antitumor effects of combining docetaxel (taxotere) with the antivascular action of ultrasound stimulated microbubbles. PLoS One 2012;7:e52307.

Gyongy M, Coussios CC. Passive cavitation mapping for localization and tracking of bubble dynamics. J Acoust Soc Am 2010;128: EL175–EL180.

Hu X, Kheirolomoom A, Mahakian LM, Beegle JR, Kruse DE, Lam KS, Ferrara KW. Insonation of targeted microbubbles produces regions of reduced blood flow within tumor vasculature. Invest Radiol 2012;47:398–405.

Idbaih A, Canney M, Belin L, Desseaux C, Vignot A, Bouchoux G, Asquier N, Law-Ye B, Leclercq D, Bissery A, De Rycke Y, Trosch C, Capelle L, Sanson M, Hoang-Xuan K, Dehais C, Houillier C, Laigle-Donadey F, Mathon B, Andre A, Lafon C, Chapelon JY, Delattre JY, Carpentier A. Safety and feasibility of repeated and transient blood−brain barrier disruption by pulsed ultrasound in patients with recurrent glioblastoma. Clin Cancer Res 2019;25:3793–3801.

Jacquart A, Keramidas M, Vollaire J, Boisgard R, Pottier G, Rustique E, Mittler F, Navarro FP, Boutet J, Coll JL, Texier I. LipImage 815: Novel dye-loaded lipid nanoparticles for long-term and sensitive in vivo near-infrared fluorescence imaging. J Biomed Opt 2013;18 101311.

Keravnou CP, De Cock I, Lentacker I, Izamis ML, Averkiou MA. Microvascular injury and perfusion changes induced by ultrasound and microbubbles in a machine-perfused pig liver. Ultrasound Med Biol 2016;42:2676–2686.

Klymchenko AS, Roger E, Anton N, Anton H, Shulov I, Vermot J, Mely Y, Vandamme TF. Highly lipophilic fluorescent dyes in nano-emulsions: Towards bright non-leaking nano-droplets. RSC Adv 2012;2:11876–11886.

Kotopoulis S, Dimcevski G, Gilja OH, Hoem D, Postema M. Treatment of human pancreatic cancer using combined ultrasound, microbubbles, and gemcitabine: A clinical case study. Med Phys 2013;40 072902.

Kurdziel KA, Kalen JD, Hirsch JI, Wilson JD, Bear HD, Logan J, McCumisky J, Moorman-Sykes K, Adler S, Choyke PL. Human dosimetry and preliminary tumor distribution of F-18-fluoropaclitaxel in healthy volunteers and newly diagnosed breast cancer patients using PET/CT. J Nucl Med 2011;52:1339–1345.

Lammers T, Kiessling F, Hennink WE, Storm G. Drug targeting to tumors: principles, pitfalls and (pre-) clinical progress. J Control Release 2012;161:175–187.

Lammertink BH, Bos C, Deckers R, Storm G, Moonen CT, Escoffre JM. Sonochemotherapy: From bench to bedside. Front Pharmacol 2015;6:138.

Lamsam L, Johnson E, Connolly ID, Wintermark M, Hayden Gephart M. A review of potential applications of MR-guided focused ultrasound for targeting brain tumor therapy. Neurosurg Focus 2018;44: E10.

Lentacker I, De Cock I, Deckers R, De Smedt SC, Moonen CT. Understanding ultrasound induced sonoporation: Definitions and underlying mechanisms. Adv Drug Deliv Rev 2014;72:49–64.

Liu HL, Fan CH, Ting CY, Yeh CK. Combining microbubbles and ultrasound for drug delivery to brain tumors: Current progress and overview. Theranostics 2014;4:432–444.

Mainprize T, Lipsman N, Huang Y, Meng Y, Bethune A, Ironside S, Heyn C, Alkins R, Trudeau M, Sahgal A, Perry J, Hynynen K. Blood−brain barrier opening in primary brain tumors with non-

invasive MR-guided focused ultrasound: A clinical safety and feasibility study. Sci Rep 2019;9:321.
Meng Y, Pople CB, Lea-Banks H, Abrahao A, Davidson B, Suppiah S, Vecchio LM, Samuel N, Mahmud F, Hynynen K, Hamani C, Lipsman N. Safety and efficacy of focused ultrasound induced blood−-brain barrier opening, an integrative review of animal and human studies. J Control Release 2019;309:25–36.
Merle P, Camus P, Abergel A, Pageaux GP, Masliah C, Bronowicki JP, Zarski JP, Pelletier G, Bouattour M, Farloux L, Dorval E, Verset G, Si-Ahmed SN, Doffoel M, Couzigou P, Taieb J, Vasseur B, Attali P. Safety and efficacy of intra-arterial hepatic chemotherapy with doxorubicin-loaded nanoparticles in hepatocellular carcinoma. ESMO Open 2017;2 e000238.
Miller KD, Nogueira L, Mariotto AB, Rowland JH, Yabroff KR, Alfano CM, Jemal A, Kramer JL, Siegel RL. Cancer treatment and survivorship statistics, 2019. CA Cancer J Clin 2019;69:363–385.
Mørch Ý, Hansen R, Berg S, Åslund AKO, Glomm WR, Eggen S, Schmid RB, Johnsen H, Kubowicz S, Snipstad S, Sulheim E, Hak S, Singh G, McDonagh BH, Blom H, Davies CdL, Stenstad PM. Nanoparticle-stabilized microbubbles for multimodal imaging and drug delivery. Contrast Media Mol Imaging 2015;10:356–366.
Mullin L, Gessner R, Kwan J, Kaya M, Borden MA, Dayton PA. Effect of anesthesia carrier gas on in vivo circulation times of ultrasound microbubble contrast agents in rats. Contrast Media Mol Imaging 2011;6:126–131.
Peer D, Karp JM, Hong S, Farokhzad OC, Margalit R, Langer R. Nanocarriers as an emerging platform for cancer therapy. Nat Nanotechnol 2007;2:751–760.
Petersen GH, Alzghari SK, Chee W, Sankari SS, La-Beck NM. Meta-analysis of clinical and preclinical studies comparing the anticancer efficacy of liposomal versus conventional non-liposomal doxorubicin. J Control Release 2016;232:255–264.
R Core Team. R: A language and environment for statistical computing. Vienna: R Foundation for Statistical Computing; 2017. Available at: https://www.R-project.org.
Raymond SB, Skoch J, Hynynen K, Bacskai BJ. Multiphoton imaging of ultrasound/Optison mediated cerebrovascular effects in vivo. J Cereb Blood Flow Metab 2007;27:393–403.
Rix A, Palmowski M, Gremse F, Palmowski K, Lederle W, Kiessling F, Bzyl J. Influence of repetitive contrast agent injections on functional and molecular ultrasound measurements. Ultrasound Med Biol 2014;40:2468–2475.
Rix A, Flege B, Opacic T, Simons N, Koczera P, Kraus K, Stickeler E, Kiessling F. Contrast enhanced ultrasound treatment enhances tumor perfusion in breast cancer patients—First results. Poster presented at the 24th European Symposium on Ultrasound Contrast Imaging. Rotterdam, The Netherlands.
Sanna V, Pala N, Sechi M. Targeted therapy using nanotechnology: Focus on cancer. Int J Nanomed 2014;9:467–483.
Schneider M. Characteristics of SonoVue. Echocardiography 1999;16:743–746.
Schneider CA, Rasband WS, Eliceiri KW. NIH Image to ImageJ: 25 years of image analysis. Nat Methods 2012;9:671–675.
Shi J, Kantoff PW, Wooster R, Farokhzad OC. Cancer nanomedicine: Progress, challenges and opportunities. Nat Rev Cancer 2017;17:20–37.
Sindhwani S, Syed AM, Ngai J, Kingston BR, Maiorino L, Rothschild J, MacMillan P, Zhang Y, Rajesh NU, Hoang T, Wu JLY, Wilhelm S, Zilman A, Gadde S, Sulaiman A, Ouyang B, Lin Z, Wang L, Egeblad M, Chan WCW. The entry of nanoparticles into solid tumours. Nat Mater 2020;19:566–575.
Snipstad S, Westrøm S, Mørch Ý, Afadzi M, Åslund AKO, Davies CdL. Contact-mediated intracellular delivery of hydrophobic drugs from polymeric nanoparticles. Cancer Nanotechnol 2014;5:8.
Snipstad S, Hak S, Baghirov H, Sulheim E, Mørch Ý, Lélu S, von Haartman E, Bäck M, Nilsson KPR, Klymchenko AS, Davies CdL, Åslund AKO. Labeling nanoparticles: Dye leakage and altered cellular uptake. Cytometry A 2017a;91:760–766.
Snipstad S, Berg S, Morch Y, Bjorkoy A, Sulheim E, Hansen R, Grimstad I, van Wamel A, Maaland AF, Torp SH, Davies CL. Ultrasound improves the delivery and therapeutic effect of nanoparticle-stabilized microbubbles in breast cancer xenografts. Ultrasound Med Biol 2017b;43:2651–2669.
Snipstad S, Sulheim E, de Lange Davies C, Moonen C, Storm G, Kiessling F, Schmid R, Lammers T. Sonopermeation to improve drug delivery to tumors: From fundamental understanding to clinical translation. Expert Opin Drug Deliv 2018;15:1249–1261.
Sulheim E, Baghirov H, von Haartman E, Bøe A, Åslund AKO, Mørch Ý, Davies CdL. Cellular uptake and intracellular degradation of poly (alkyl cyanoacrylate) nanoparticles. J Nanobiotechnology 2016;14:1.
Sulheim E, Iversen TG, To Nakstad V, Klinkenberg G, Sletta H, Schmid R, Hatletveit AR, Wagbo AM, Sundan A, Skotland T, Sandvig K, Morch Y. Cytotoxicity of poly(alkyl cyanoacrylate) nanoparticles. Int J Mol Sci 2017;18:2454.
Sulheim E, Morch Y, Snipstad S, Borgos SE, Miletic H, Bjerkvig R, Davies CL, Aslund AKO. Therapeutic effect of cabazitaxel and blood-brain barrier opening in a patient-derived glioblastoma model. Nanotheranostics 2019;3:103–112.
van Wamel A, Healey A, Sontum PC, Kvale S, Bush N, Bamber J, Davies CdL. Acoustic Cluster Therapy (ACT) - pre-clinical proof of principle for local drug delivery and enhanced uptake. J. Control. Release 2016a;224:158–164.
van Wamel A, Sontum PC, Healey A, Kvåle S, Bush N, Bamber J, Davies CdL. Acoustic Cluster Therapy (ACT) enhances the therapeutic efficacy of paclitaxel and Abraxane for treatment of human prostate adenocarcinoma in mice. J. Control. Release 2016b;236:15–21.
Wang Y, Li Y, Yan K, Shen L, Yang W, Gong J, Ding K. Clinical study of ultrasound and microbubbles for enhancing chemotherapeutic sensitivity of malignant tumors in digestive system. Chin J Cancer Res 2018;30:553–563.
Wilhelm S, Tavares AJ, Dai Q, Seiichi O, Audet J, Dvorak HF, Chan WCW. Analysis of nanoparticle delivery to tumours. Nat Rev Mater 2016;1:1–12.
Wood AK, Ansaloni S, Ziemer LS, Lee WM, Feldman MD, Sehgal CM. The antivascular action of physiotherapy ultrasound on murine tumors. Ultrasound Med Biol 2005;31:1403–1410.
Wu J, Zhang J, Jiang M, Zhang T, Wang Y, Wang Z, Miao Y, Wang Z, Li W. Comparison between NOD/SCID mice and BALB/c mice for patient-derived tumor xenografts model of non-small-cell lung cancer. Cancer Manag Res 2018;10:6695–6703.
Yemane PT, Aslund AKO, Snipstad S, Bjorkoy A, Grendstad K, Berg S, Morch Y, Torp SH, Hansen R, Davies CL. Effect of ultrasound on the vasculature and extravasation of nanoscale particles imaged in real time. Ultrasound Med Biol 2019;45:3028–3041.